Spatial Frequency Domain Imaging of Port Wine Stain Biochemical Composition in Response to Laser Therapy: A Pilot Study

Amaan Mazhar, PhD,[1] Seyed A. Sharif, MD,[1] J. David Cuccia, PhD,[2] J. Stuart Nelson, MD, PhD,[1,3,4] Kristen M. Kelly, MD,[1,3] and Anthony J. Durkin, PhD[1,3]*

[1]*Beckman Laser Institute, University of California, Irvine, California 92612*

[2]*Modulated Imaging Inc., Technology Incubator Office, 1002 Health Sciences Road East, Irvine, California 92612*

[3]*Department of Surgery, University of California, Irvine, California 92612*

[4]*Department of Biomedical Engineering, University of California, Irvine, California 92612*

Background and Objective: Objective methods to assess port wine stain (PWS) response to laser treatment have been the subject of various research efforts for several years. Herein, we present a pilot study using a newly developed, light emitting diode (LED) based spatial frequency domain imaging (SFDI) device to record quantitatively biochemical compositional changes in PWS after laser therapy.

Study Design/Patients and Methods: A SFDI system was used to image before, and after, five PWS treatment sessions [$n = 4$ subjects (one subject was imaged before and after two consecutive laser treatments)]. SFDI derived wide-field optical properties (absorption and scattering) and tissue chromophore concentrations including oxy-hemoglobin (ctO_2Hb), deoxy-hemoglobin (ctHHb), total hemoglobin (ctTHb), and tissue oxygen saturation (stO_2) are presented for skin imaged prior to and immediately after laser treatment. The SFDI derived images were analyzed by comparing the above measurements in PWS to those of normal skin and tracking changes immediately after laser exposure.

Results: Elevated oxy-hemoglobin (>20%) and tissue oxygen saturation (>5%) were measured in all PWS lesions and compared to values for normal skin prior to treatment. Laser treatment resulted in an increase in deoxy-hemoglobin (>100%), decrease in tissue oxygen saturation (>10%), and reduced scattering (>15%) in all PWS lesions. One subject was followed before and after two consecutive laser treatments and the overall improvement in PWS lesion blanching was quantitatively assessed by measuring a 45% decrease in dermal blood volume.

Conclusion: SFDI is a rapid non-contact wide-field optical technique that shows potential as an imaging device that can be used to quantify biochemical compositional changes in PWS after laser therapy. Future work will investigate the potential of SFDI to provide intra-operative guidance for laser therapy of PWS lesions on an individual patient basis. Lasers Surg. Med.

Key words: port-wine stains; modulated imaging; spatial frequency domain imaging; multispectral imaging

INTRODUCTION

Port wine stain (PWS) birthmarks are congenital progressive vascular malformations that typically occur on the head or neck [1]. These lesions are difficult to conceal and are often the cause of physical and emotional disability due to facial asymmetry and deformity [2]. Pulsed dye laser (PDL) therapy with epidermal cooling is the current standard approach to treat these birthmarks by enabling destruction of abnormal subsurface blood vessels without significant damage to the epidermis.

In PDL therapy, light (typically 585–595 nm) is preferentially absorbed by hemoglobin to induce selective photothermolysis of the blood vessels [3]. Dynamic cooling is coupled with treatment to minimize heat generation in the epidermis, which can lead to scarring or dyspigmentation. However, PWS blood vessel size, density, and depth is highly variable on an individual patient basis and even from site to site on the same patient. Thus, PWS blanching in response to laser therapy can be unpredictable. During PWS laser-treatment, the surgeon will methodically move the hand piece over the entire birthmark. Due to the heterogeneity of blood vessel geometry in PWS lesions, it is often difficult to assess treatment efficacy. The onset of purpura (i.e., bluish-gray skin discoloration)

Conflict of Interest Disclosures: All authors have completed and submitted the ICMJE Form for Disclosure of Potential Conflicts of Interest and have disclosed the following: Dr. Cuccia and Dr. Durkin are co-founders of Modulated Imaging Inc.

Contract grant sponsor: National Institute of Health, Armed Forces Office of Scientific Research, Beckman Foundation; Contract grant numbers: R43RR030696-01A1, R43-RR025985-01, P 41-RR01192, AR59244, AR4755, FA9550-08-1-0384.

*Corresponding to: Anthony J. Durkin, PhD, Beckman Laser Institute, 1002 Health Sciences Road East, Irvine, CA 92617.
E-mail: adurkin@uci.edu

Accepted 25 July 2012
Published online in Wiley Online Library (wileyonlinelibrary.com).
DOI 10.1002/lsm.22067

© 2012 Wiley Periodicals, Inc.

is often used by the surgeon as a visual clue of the clinical endpoint. Purpura occurs when a PWS blood vessel is ruptured irreversibly by laser exposure and red blood cells extravasate into the surrounding perivascular space. However, the utility of purpura as a clinical endpoint remains incompletely understood.

PWS treatment is currently a subjective procedure due to choices in laser device, light dosage, wavelength, pulse duration, and treatment frequency resulting in variable success rates. There is an unmet need for technologies which can determine quantitative metrics that will help inform and assess treatment protocols for PWS management. Several optical instruments have been investigated as quantitative measures of PWS laser treatment efficacy. Methods such as optical Doppler tomography (ODT) [4], laser Doppler flowmetry imaging (LDFI) [5], and laser speckle imaging (LSI) measure tissue perfusion [6]. Other methods such as reflectance spectroscopy [7] and cross-polarized diffuse reflectance imaging [8] measure intrinsic absorption in tissue. All of the aforementioned methods attempt to determine PWS blood vessel depth, size, flow, and distribution in human skin before and after laser exposure. "Each technology has its own unique advantages and disadvantages. However, none of the technologies mentioned has become part of the standard of care for PWS treatment. ODT and LDFI measure flow/perfusion in tissue but are susceptible to motion artifacts and limited to small fields of view due to long scan times. LSI is another flow/perfusion imaging method amenable to wide-field imaging but measures superficial volumes (<1 mm) and measures relative changes in flow as it can be affected by changes in optical properties. Reflectance spectroscopy is typically a probe-based measurement and thus cannot provide high resolution images unless the sources are scanned. Multi-spectral cross-polarized imaging methods measure tissue chromophores but do not directly measure the scattering in tissue which can be a unique signal to measure breakdown of cells after treatment. Thus, there is a need for a rapid wide-field imaging technology that can rapidly measure subsurface tissue biochemical composition (absorption) as well as structural information (scattering) over large areas."

Herein, we present initial measurements of PWS patients using spatial frequency domain imaging (SFDI)—a non-contact, wide-field imaging method [9,10] which uses structured illumination coupled with a light propagation model to measure intrinsic tissue optical properties. The resulting data products are two-dimensional maps of absorption (μ_a) and reduced scattering (μ_s') at discrete wavelengths. Combined with multi-spectral imaging at optimal wavelengths, this method is able to characterize tissue biochemical composition by quantitatively mapping oxy-hemoglobin (ctO_2Hb), deoxy-hemoglobin (ctHHb), total hemoglobin (ctTHb), and tissue oxygen saturation (stO_2) [11]. Multi-spectral imaging has been used extensively to measure tissue oxygen saturation and blood volume in skin applications [12,13]. However, SFDI is unique as it can also quantify the reduced scattering coefficient which can give insight into structural changes in tissue. SFDI has been previously used to measure chromophores in volar forearm [9,11], optical properties of tattooed skin [14], as well as pre-clinical and clinical tissue transfer flaps [15–17]. We will also present a pilot study to demonstrate the capabilities of a new, light emitting diode (LED) based SFDI to characterize the biochemical composition of PWS human skin before and after laser therapy.

MATERIALS AND METHODS

Spatial Frequency Domain Imaging (SFDI) Method

The theory behind tissue optical property characterization and imaging in the spatial frequency domain has been described [9]. Briefly, SFDI uses spatially modulated structured illumination patterns projected (Fig. 1a) onto tissue at various frequencies in the form:

$$S = \frac{S_0}{2}[1 + M_0 \cos(2\pi f_x + \alpha)] \tag{1}$$

where S_0, M_0, f_x, and α are the illumination source intensity, modulation depth, spatial frequency, and spatial phase, respectively. The remitted light, I, from the sample is captured by a CCD camera and is composed of AC and DC components

$$I = I_{AC} + I_{DC} \tag{2}$$

The measured AC component of the remitted intensity, I_{AC}, can be characterized as:

$$I_{AC} = M_{AC}(x, f_x) \times \cos(2\pi f_x + \alpha) \tag{3}$$

where $M_{AC}(x, f_x)$ represents the modulation of diffusively reflected photon density waves (PDW) which in turbid media depend on the optical properties of the tissue and can be modeled with diffusion based or Monte Carlo based light transport methods [9]. In order to extract $M_{AC}(x, f_x)$, a signal demodulation method is used. The sample is illuminated with a sinusoidal pattern at a specific spatial frequency with three phase offsets $\alpha = 0$, $2\pi/3$, and $4\pi/3$ radians (Fig. 1a). $M_{AC}(x, f_x)$ is then calculated using the demodulation expression:

$$M_{AC}(x, f_x) = \frac{\sqrt{2}}{3}\left[(I_1 - I_2)^2 + (I_2 - I_3)^2 + (I_3 - I_2)^2\right]^{1/2} \tag{4}$$

In order to calculate tissue optical properties, $M_{AC}(x, f_x)$ can be measured using three phase projection images at a high spatial frequency ($f_x > 0.1$ mm^{-1}) and planar illumination or low spatial frequency ($f_x = 0$ mm^{-1}). First, multiple-frequency patterns are projected over the sample (Fig. 1a). The patterns are projected at multiple phases over the sample and demodulated using Equation (4) (Fig. 1b). The diffuse reflectance is then calculated at each spatial frequency using a silicone calibration phantom of known optical properties (Fig. 1b). This calibration step

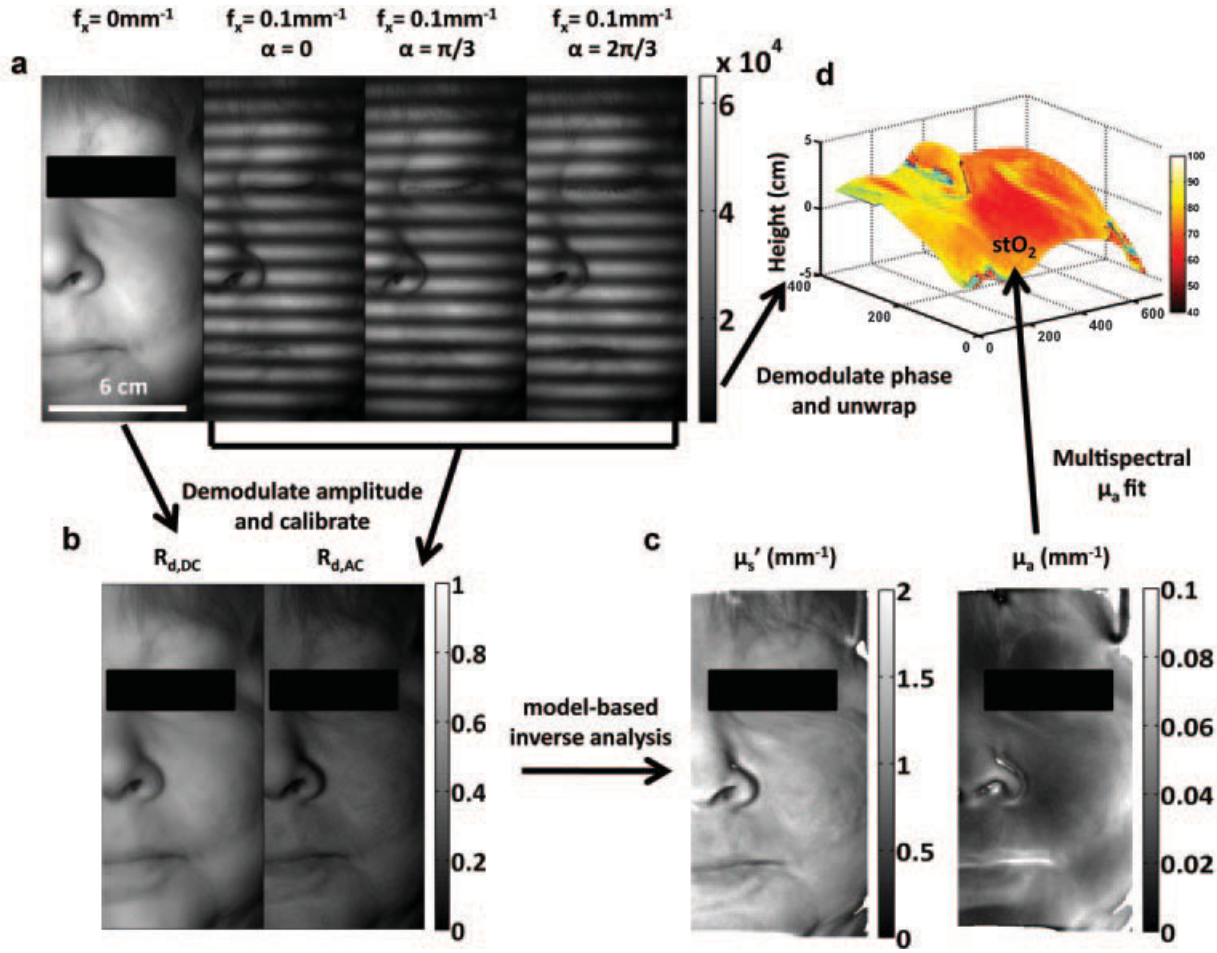

Fig. 1. Data flow in SFDI. **a**: Patterns are projected onto tissue sample and then (**b**) demodulated and calibrated to a known standard. **c**: A pre-calculated look-up table is then used to derive tissue optical properties on a pixel by pixel basis.

allows us to correct for the modulation transfer function (MTF) of the system which can be affected by spatial variation of the illumination light and net throughput of system optical components. Finally, an inverse model fit is applied to each pixel in the image in order to generate optical property maps at a discrete wavelength (Fig. 1c). The sample height is calculated using sinusoid phase information (Fig. 1d). Height maps can then be applied to correct the reflectance using an algorithm described previously [18]. This correction algorithm uses a calibration scheme based on multiple calibration phantoms to correct for intensity changes due to vertical translation in height and variations in surface angles. The present study utilizes a single AC high spatial frequency (0.1 mm^{-1}) measurement combined with a low frequency DC measurement (0 mm^{-1}) to calculate μ_a and μ_s'. These data are then compared to a known look-up table (LUT) created with a known forward Monte Carlo model [9]. The LUT allows for relatively rapid visualization of the data (~10 seconds).

In order to measure intrinsic biological chromophores such as oxy- and deoxy-hemoglobin, the scattering corrected optical absorption maps are measured at discrete wavelengths using SFDI. In general, the optical absorption at a single wavelength, μ_a, can be characterized by:

$$\mu_a(\lambda_i) = \sum_{n=1}^{N} \varepsilon_n(\lambda_i) c_n \tag{5}$$

where μ_a, $\varepsilon_n(\lambda_i)$, c_n, and N represent the optical absorption coefficient, chromophore extinction coefficient at a given wavelength, chromophore concentration, and number of chromophores, respectively. With a priori knowledge of the extinction coefficient matrix, $\varepsilon_n(\lambda_i)$ and measurements of the absorption coefficient at multiple wavelengths, the concentration, c_n, of each chromophore can be extracted using Equation (5). Typical basis spectra for tissue chromophores have been measured and characterized by multiple researchers and are used here [19].

SFDI Instrumentation

A typical SFDI instrument consists of three fundamental components: a light source, spatial light modulator, and camera. For these studies, a prototype clinic-compatible system (Modulated Imaging Inc., Irvine, CA) was used to measure tissue oxy-hemoglobin (ctO_2Hb), deoxy-hemoglobin (ctHHb), and tissue oxygen saturation (stO_2). The imaging head is contained in a compact enclosure ($\sim 7' \times 8' \times 11'$) and light-weight ($\sim$12 lb) enough to be mounted on an articulating arm attached to a portable cart which also houses a computer and isolation transformer (Tripplite, Chicago, IL) for electrical safety reasons (Fig. 2a). The system is designed to image a 13.5 cm $\times$ 10.5 cm field of view at a working distance of 18.5 cm from the front of the imaging box. As explained above, the SFDI system must have multi-spectral imaging capabilities to extract tissue chromophore concentrations. Based on previous work [11], a light source consisting of modules with LED's (Innovations in Optics, Woburn, MA) centered at 658, 730, 850, and 970 nm have been implemented in this system to optimize quantification of the chromophores listed above [11]. The full widths at half maximum's (FWHM) of these LED's are approximately 16, 23, 24, and 35 nm, respectively. LED temperatures and intensities are stabilized with thermoelectric cooling (TEC) built into the system and the delivered light power at the tissue surface is <1 mW/cm^2 for each LED wavelength. A digital light projector based on a Digital Micromirror Device (Texas Instruments DMD Discovery^{TM} 1100) is used to project patterns onto sample. Two co-registered cameras (Lumenera, Canada) are employed including a dedicated near-infrared (NIR) camera for SFDI imaging and a color camera for capturing clinical impression (Fig. 2b). White light is projected after each pass of data to capture a color photograph of the region of interest so that SFDI data can be compared at the exact same site on human skin before and after laser treatment. The projector and NIR detection arms are fitted with cross-polarizers to eliminate specularly reflected photons. All system hardware is controlled by custom C# software (Modulated Imaging Inc., Irvine, CA) connected to a PC computer via universal serial bus (USB). In addition to SFDI data, a surface profilometry measurement is built into the acquisition in order to correct or optical property errors resulting from surface curvature, as described by Gioux et al. [18]. The design and stability testing of this system has been described in phantoms [20,21]. Optical property determination, chromophore concentration map rendering, and image processing are done using MATLAB (the MathWorks, Natick, MA), which occurs off-line, after data have been acquired.

Imaging of PWS Skin

Four PWS subjects were recruited from an outpatient population at the Beckman Laser Institute and Medical Clinic, University of California, Irvine (UCI) in compliance with IRB approved protocol #2010-7276 (Table 1). Informed consent was obtained from all subjects. All PWS lesions were located on the face and subjects were asked to lie down supine on a gurney prior to measurement in order to minimize motion artifacts. Motion during measurements can result in demodulation artifacts (Equation 4) and subsequent errors in optical property inversion. Thus, rapid imaging and minimization of motion was crucial [22]. Each PWS lesion was measured prior to, and immediately, after laser treatment. Laser parameters for each patient were chosen by the treating surgeon and summarized in Table 1. Two lasers were used to treat PWS lesions on the subjects enrolled in this study: V-beam Perfecta 595 nm PDL (Syneron/Candela Laser

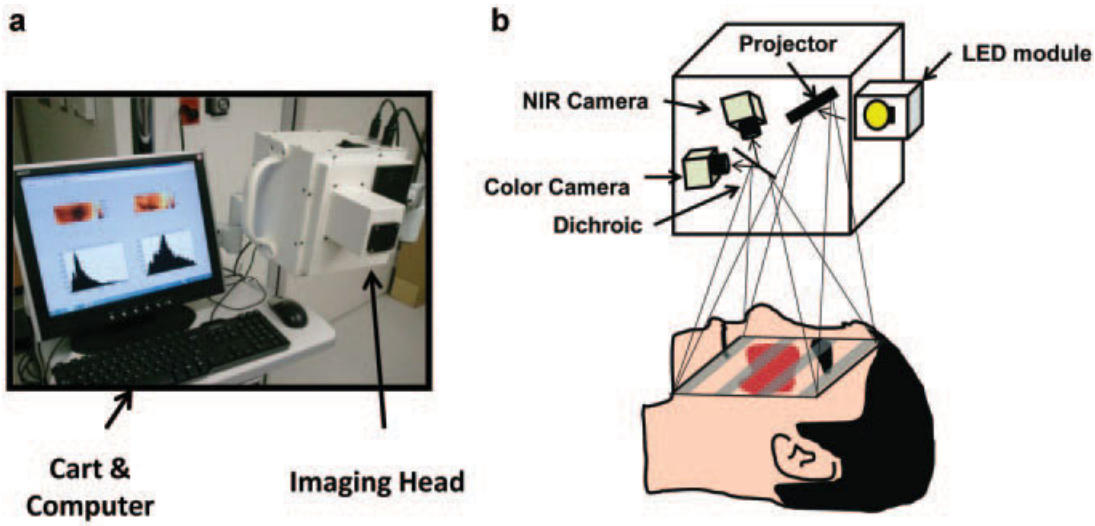

Fig. 2. **a**: A compact and lightweight LED-based instrument used for the clinical measurements described herein. **b**: A typical SFDI system consists of three fundamental components: a light source, a spatial light modulator, and a camera.

TABLE 1. Summary of Information Related to Laser Treatment for Subjects 1–4

Measurement	Gender	Age (years)	Laser wavelength (nm)	Spot size (mm)	Laser dosage (J/cm^2)	Pulse duration (milliseconds)	Cryogen cooling (spurt (milliseconds), delay (milliseconds))	Treated area
1a	F	65	755	10	60	3	30/30	Left cheek 70 cm^2
			595	7	10	1.5	30/30	
			595	12	6.25	0.45	30/30	
1b	F	65	755	10	60	3	30/30	Left cheek 70 cm^2
			595	12	6.5	0.45	30/30	
			595	10	10	3	30/30	
2	F	12	595	10	10	1.5	30/30	Left face 160 cm^2
			595	12	6.5	0.45	30/30	
3	M	26	755	10	60	3	50/30	Right face 170 cm^2
			595	10	10	3	30/30	
4	M	37	595	10	10	1.5	30/30	Left face 250 cm^2

Subject 1 was Imaged on Two Different Occasions; Hence 1a, 1b

Corporation, Wayland, MA) and the GentleLASE 755 nm alexandrite laser (Syneron/Candela Laser Corporation, Wayland, MA). All post-operative measurements were taken before application of post-treatment topical medications (Aloe vera gel), which potentially interfere with the measurement. The delay was less than 5 minutes in each case and patients were not in severe pain during this delay and remained under the observation of the clinician. Aloe vera is applied to reduce post-treatment discomfort and the small delay in application does not affect treatment outcome as determined by the clinician.

SFDI data was acquired at all four LED wavelengths (658, 730, 850, and 970 nm) using five spatial frequencies spaced evenly between 0 and 0.2 mm^{-1}. Three repetitions of data were taken during each 25-second measurement. Only two frequencies (0 and 0.1 mm^{-1}) were used to process the data so that the impact of motion artifacts could be minimized. SFDI data were processed using a height correction algorithm described previously [18]. This correction algorithm uses a multiple phantom calibration to correct for intensity changes due to vertical translation in height and variations in surface angles which accounts for the largest source of error ion reflectance (up to 15% changes in reflectance for a 2 cm variation). A one layer Monte Carlo model of light propagation in the spatial frequency domain was used, allowing analysis of reflectance for a wide span of optical properties. We have shown in previous work that absorption and scattering maps can be rapidly determined by measuring reflectance at two spatial frequencies using a pre-computed LUT, a computational optimization of a 2-frequency nonlinear least-squares model-based analysis [9].

RESULTS

Wide-Field Mapping of PWS Chromophore Concentrations

SFDI derived optical property data and chromophore concentration data for subject 1 measured on the PWS as compared to normal skin are shown in Figure 3. To the best of our knowledge, these results are the first reported wide-field maps of PWS optical properties and chromophore concentrations. We can extract mean optical properties and chromophore values by averaging the pixel values of specific regions of interest (ROI) that correspond to normal and PWS skin in the extracted SFDI maps. The regions used for analysis in all maps for subject 1 are shown with white and black boxes in the color image respectively (Fig. 3a). Pre-treatment optical properties show that the absorption coefficient on the PWS (0.045 mm^{-1}) is greater than the surrounding normal skin (0.037 mm^{-1}) at 658 nm. Before laser treatment, ctTHb (which is analogous to blood volume) associated with PWS skin is actually elevated compared to normal skin (220 μM vs. 114 μM) as is stO_2 (84.5% vs. 67.2%). Color images show the purpura that develops after laser treatment (Fig. 3a). The mean absorption coefficient in the PWS lesion increases to 0.12 mm^{-1} at 658 nm after treatment (Fig. 3b) and the reduced scattering decreases from 1.35 to 1.12 mm^{-1} (Fig. 3c). The absorption increase at 658 nm due to treatment is strongly correlated with a mean increase in ctHHb (Fig. 3d) from 34 to 123 μM and ctTHb (Fig. 3e) from 220 to 317 μM. The mean stO_2 in the PWS decreases dramatically after laser treatment from 84.5% to 61.4% (Fig. 3f). The mean chromophore values of the PWS lesion for subject 1 before and after laser treatment are summarized in Table 2. It is important to note that these are mean values from a selected ROI and do not represent the heterogeneity of the data which is evident by the standard deviations associated with the ROIs.

SFDI Measures Reduced Blood Volume in Blanched PWS

Subject 1 was studied before and after two consecutive laser treatments. There was an interval of 2 months between the two laser treatments. Prior to the second laser treatment, the PWS visually appeared less red (i.e.,

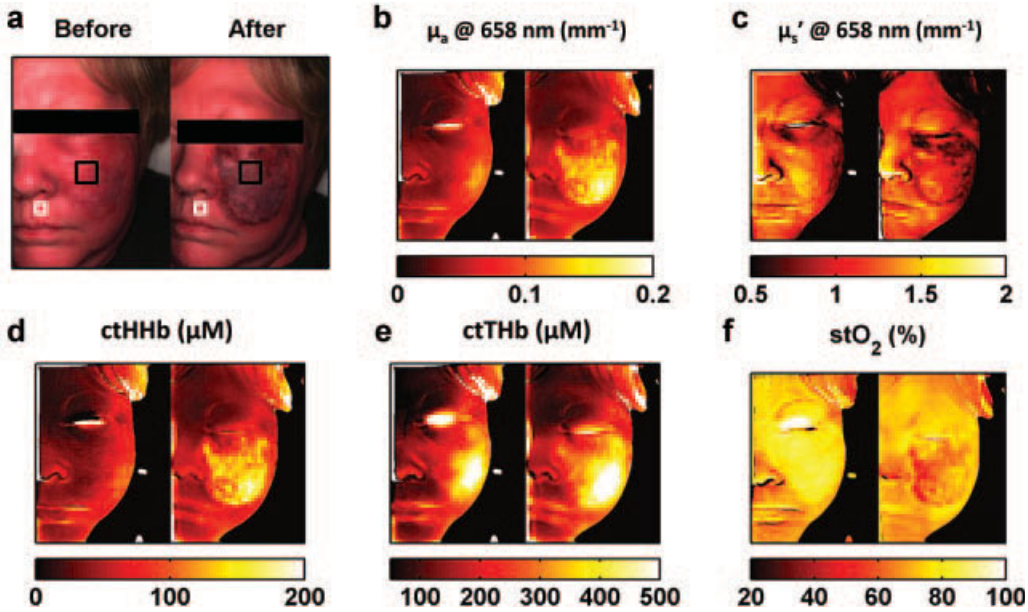

Fig. 3. SFDI derived PWS data for subject 1 (measurement 1a). Collage of pre-operative (**left**) and postoperative (**right**) (**a**) color images, t (**b**) absorption map, (**c**) scattering map, (**d**) deoxy-hemoglobin maps, (**e**) total hemoglobin, and (**f**) tissue oxygen saturation. Elevated ctTHb and stO_2 (relative to surrounding normal skin) are seen in lesion prior to laser treatment. An increase in ctHHb, ctTHb, and decrease in stO_2 (relative to pre-treatment concentrations) is evident immediately after treatment.

blanched) as compared to baseline (Fig. 4a). The baseline mean values of ctTHb in the PWS were also lower at the second visit (133 μM) as compared to the first visit (220 μM), although still higher than normal skin (82 μM). The PWS skin to normal skin ratio of ctTHb was also lowered (1.93 vs. 1.62) between visits. Before treatment, mean stO_2 in the PWS was also elevated compared to normal skin (86.1% vs. 64.6%). The second treatment showed the same trends in optical property and chromophore changes as compared to the first treatment but with lower magnitudes of change. The mean absorption coefficient in the PWS lesion increased from 0.026 to 0.055 mm^{-1} at 658 nm after treatment (Fig. 4b) and the reduced scattering decreased from 1.37 to 1.10 mm^{-1} (Fig. 4c). The absorption increase at 658 nm after treatment is strongly correlated with a mean increase in ctHHb (Fig. 4d) from 18 to 50 μM and ctTHb (Fig. 4e) from 133 to 182 μM. The mean stO_2 in the PWS decreases dramatically after laser treatment from 86.1% to 74.2% (Fig. 4f). The mean chromophore values of the PWS lesion on subject 1 before and after both laser treatment are also summarized in Table 2. Additionally, it is apparent in the maps that the spatial heterogeneity of stO_2 changes due to treatment is more diverse compared to the previous visit which is confirmed by the larger standard deviation in the ROI. Although we compare normalized values of chromophores and optical properties for each visit, it is important to note that the value of stO_2 for normal skin between visits (67% vs. 65%) is quite similar.

Elevated ctO_2Hb and stO_2 in PWS Skin Prior to Treatment

Similar ROI analysis was carried out on a total of five subject's PWS before and after laser treatment. SFDI derived stO_2 maps are shown for patients 2–4 (Fig. 5a–c). An ROI on the PWS and normal skin was selected as for the previous subject. Changes in PWS lesion biochemical composition and optical properties at 658 nm are

TABLE 2. Mean PWS Chromophore Values for Subject 1 Before and After Laser Treatment

Measurement	ctO_2Hb (μM)	ctHHb (μM)	ctTHb (μM)	stO_2 (%)	μ_a (658 nm) (mm^{-1})	μ_s' (658 nm) (mm^{-1})
1a: Pre-treatment	186 ± 14	34 ± 4	220 ± 12	84.5 ± 2.0	0.045 ± 0.003	1.35 ± .06
1a: Post-treatment	194 ± 17	123 ± 13	317 ± 18	61.4 ± 3.7	0.119 ± 0.01	1.12 ± .09
1b: Pre-treatment	115 ± 13	18 ± 1	133 ± 13	86.1 ± 1.2	0.026 ± 0.002	1.37 ± .06
1b: Post-treatment	143 ± 13	50 ± 11	193 ± 7	74.2 ± 5.8	0.055 ± 0.008	1.10 ± 0.10

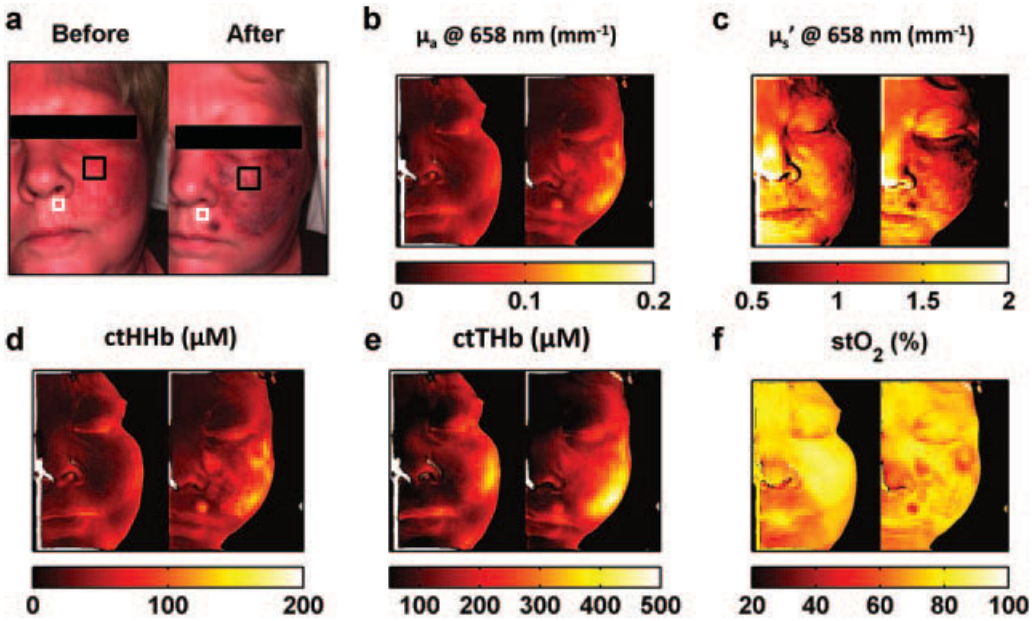

Fig. 4. SFDI derived PWS data for subject 1 after subsequent visit (measurement 1b). Collage of pre-operative (**left**) and postoperative (**right**) (**a**) color images, *t* (**b**) absorption map, (**c**) scattering map, (**d**) deoxy-hemoglobin maps, (**e**) total hemoglobin, and (**f**) tissue oxygen saturation. Elevated ctTHb and stO_2 (relative to surrounding normal skin) was seen in lesion prior to laser treatment. An increase in ctHHb, ctTHb, and decrease in stO_2 is evident immediately after treatment. However, the treatment area changes are not as uniform or dramatic as compared to previous visit.

summarized in Table 3. Mean optical properties (shown with ranges) for normal skin, PWS pre-treatment and PWS post-treatment are shown at each measured wavelength (Fig. 6). In general, there is a mean increase in absorption (blood pooling) and a mean decrease in scattering (structural changes) in PWS post-treatment. The mean chromophore and scattering values of the PWS lesion were then divided by mean values of normal skin and plotted (Fig. 7a). In general, PWS lesions show elevated ctO_2Hb (>15%), ctTHb (>15%), and stO_2 (>5%) as compared to normal skin before laser treatment.

Elevated ctTHb and Decreased stO_2 in PWS Skin Post Treatment

A similar ROI was selected on each subject for the PWS lesion post laser treatment. SFDI derived chromophore concentration and reduced scattering coefficient values of a PWS lesion after laser treatment were divided by normal skin post-treatment. This ratio was then divided by the ratio of lesion and normal skin prior to treatment to reveal changes due to treatment (Fig. 7b). Immediately after laser treatment, all PWS lesions showed a dramatic

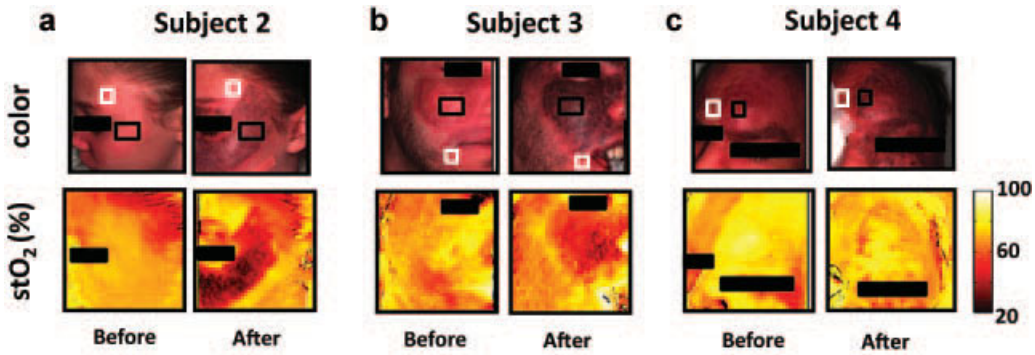

Fig. 5. Color images and SFDI derived stO_2 maps for subjects 2–4 before and after PDL treatment.

TABLE 3. Mean PWS Chromophore Values for Subjects 2–4 Before and After Laser Treatment

Measurement	ctO_2Hb (μM)	ctHHb (μM)	ctTHb (μM)	stO_2 (%)	μ_a (658 nm) (mm^{-1})	μ_s' (658 nm) (mm^{-1})
2: Pre-treatment	83 ± 5	30 ± 3	113 ± 7	73.1 ± 1.7	0.032 ± 0.004	1.31 ± 0.04
2: Post-treatment	63 ± 5	92 ± 9	154 ± 9	40.7 ± 3.6	0.08 ± 0.007	1.07 ± 0.07
3: Pre-treatment	134 ± 9	53 ± 6	188 ± 12	71.5 ± 2.2	0.057 ± 0.005	1.39 ± 0.1
3: Post-treatment	192 ± 33	169 ± 17	361 ± 46	53.0 ± 3.3	0.156 ± 0.016	0.89 ± 0.06
4: Pre-treatment	309 ± 12	81 ± 7	389 ± 15	79.3 ± 1.6	0.094 ± 0.006	1.18 ± 0.07
4: Post-treatment	280 ± 24	156 ± 37	436 ± 56	64.8 ± 4.9	0.152 ± 0.032	1.18 ± 0.10

increase (>100%) in ctHHb and (>10%) ctTHb concentration. This coincided with decreases in stO_2 (>10%) and reduced scattering coefficient (>15%) compared to normal skin.

DISCUSSION

We have presented SFDI within the context of PWS biochemical composition/assessment prior to, and immediately after, laser treatment. First, functional chromophore and reduced scattering coefficient maps can be used to quantify redness and lesion extent which can help follow PWS response to laser therapy. Prior to treatment, elevated tissue oxygen saturation was evident in each PWS as compared to surrounding normal skin. Elevated tissue oxygen saturation suggests higher values of oxy-hemoglobin relative to deoxy-hemoglobin which explains the visual redness observed in a PWS lesion. Another optical index, the erythema index, has been shown to have elevated values in PWS lesions [23] and is a measurement of hyperemia as compared to normal skin and is consistent with the concept of elevated tissue oxygen saturation that we observed. The link between elevated tissue oxygen saturation and clinical characteristics of PWS is unclear but a double blinded study that correlates clinical evaluation with stO_2 could identify utility of this quantitative metric.

Additionally, all four PWS lesions showed elevated blood volumes as compared to normal skin. Previous work has also shown that lower light dosages can induce purpura in PWS that have dilated blood vessels characterized by higher dermal blood volume fractions [24]. In this case, a PWS with a greater blood volume may require a less aggressive treatment protocol. In general, light dosage and pulse duration are often selected by surgeons based on redness or PWS blood vessel density. Thus, the SFDI derived total blood volume in PWS lesions has the potential to inform the surgeon in the treatment planning stage by helping decide correct laser dosage and pulse width. Optimal parameter selection could help to achieve better PWS blanching while minimizing adverse effects. The current pilot study showed a dramatic increase in ctHHb within PWS lesions after laser treatment. This occurs when the vasculature is compromised and red blood vessels leaks into the surrounding perivascular tissue. Purpura is a subjective visual sign used by surgeons to determine the endpoint of a single PWS lesion treatment. However, there is debate on the amount of purpura that

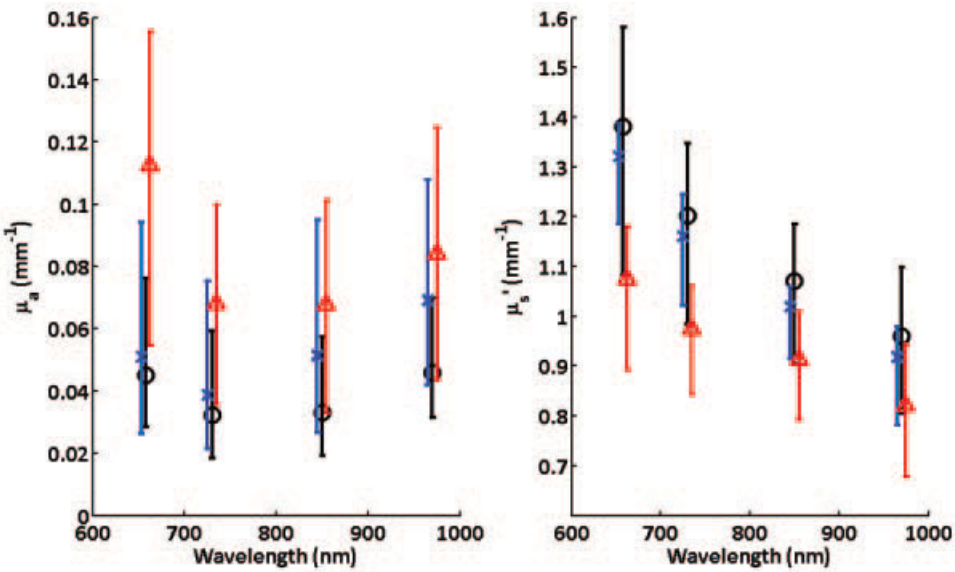

Fig. 6. Optical property summary (mean + range) of normal and PWS skin for subjects 1–5 before and after PDL treatment.

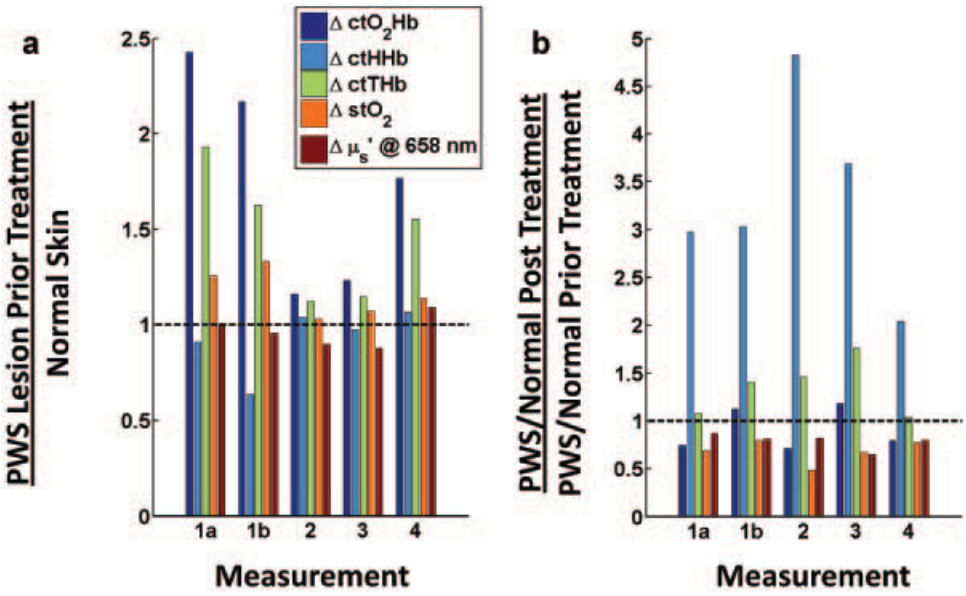

Fig. 7. Summary of chromophore concentration changes in four subjects. **a**: All PWS lesions show elevated values of ctO_2Hb, stO_2, and μ_s' as compared to surrounding normal skin; (**b**) treatment results in increases in ctHHb, ctTHb, and decreases in stO_2 and μ_s' compared to pre-treatment measurements. Horizontal line represents a ratio of one between reported values.

is required for a successful response to laser therapy in terms of lesion blanching. A SFDI generated map of acute biochemical composition changes potentially may be a quantitative tool to determine the treatment endpoint in a wide-field manner. For example, the second treatment for subject 1 resulted in changes in chromophores and stO_2 that were not uniform across the whole lesion and could inform the surgeon of the immediate need for retreatment. Also, this technology shows potential as a quantitative measure of PWS blanching to assess efficacy of a long-term treatment plan. A more detailed, larger scale study is needed to correlate the particular quantitative changes associated with an effective or "optimal" treatment.

Optimization of SFDI acquisition parameters (acquire only essential frequencies), hardware components (implementation of graphics processor units), and software improvement (lookup table algorithm) improvement can potentially reveal any inconsistencies in treatment in near real time ($\sim$1 frame/second). This type of visualization rates can aid surgeons by providing immediate feedback on which areas may need retreatment during the procedure. Surgeons methodically treat large lesions but frequently a laser pulse at a particular location may be ineffective due to PWS blood vessel heterogeneity. The before and after treatment images in Figures 3 and 4 clearly show the heterogeneity of changes spatially between visits.

It is important to note the variability in reduced scattering coefficient measured here using SFDI in PWS lesions. SFDI is different from traditional multi-spectral imaging techniques as it separates absorption from scattering using structured illumination which allows improved measurement of chromophores. Reduced scattering coefficient is a strong correlate to structural changes as it is a function of the distribution and size of scattering objects such as collagen fibrils in tissue [25]. Thus, there may be a relationship between the scattering maps and measuring the onset of hypertrophic scarring. Further elucidation of this relationship will be the subject of a future study.

Further improvements in SFDI data processing may be achieved in the future by implementing a more sophisticated model. For example, a two-layer model may be used in order to account for the effect of epidermal melanin absorption on the SFDI derived ctO_2Hb and ctHHb concentrations [26]. Melanin can be a confounding factor for measurements between sessions to assess treatment response, resulting in artificially low values of oxy- and deoxy-hemoglobin concentrations. The results of the study presented here were minimally affected by epidermal melanin concentration as it involved only Caucasian subjects with relatively light skin photo-types as compared to other ethnicities. It is also important to note that the analysis methods used in this study measure volume averaged absorption and scattering properties. A dramatic increase in absorption values (such as the 10-fold increase observed in laser treated skin) would result in a more superficial average interrogation volume by the light. In both of these cases, MI is still interrogating the dermal layer of the skin when using NIR light. However, the relative contribution of dermal (i.e., papillary vs.

reticular) layers may vary between patients and measurements. Although, the current methods have shown some contrast to blood volume changes, a more advanced model that incorporates layers may help differentiate changes that are depth and layer specific [14]. In reality, tissue is more complex than this and it is desirable to increase the degree of sophistication of the models that we use to deduce information. For example, SFDI is amenable to multi-layer modeling approaches which suggests that a melanized layer overlying a dermis-like substrate may be the next step in terms of increasing the generality of the approach so that it is amenable to include darker skin types [27–29]. Finally, another area of potential refinement is with regard to improvement of visualization and rendering time of data. These SFDI data were processed off-line in a few minutes after the data are acquired. Graphics Processing Units (GPUs) have the potential to enable real-time visualization, as treatment is occurring. This GPU based approach has been effectively used to this effect for visualization of therapy specific treatment information associated with other imaging modalities [30]. Efforts have begun to use this approach for SFDI data which would truly enable the technology for the purposes of intra-operative guidance.

This pilot study has illustrated the potential of SFDI to render wide-field biochemical composition of tissue health by measuring tissue chromophore concentrations before and after laser treatment of PWS lesions. Larger scale, more detailed studies are needed to assess the impact of SFDI-derived information to either guide treatment in real time and/or predict PWS response to laser therapy.

DISCLOSURE OF PROPRIETARY INTERESTS

There is no financial interest or commercial association for Amaan Mazhar, PhD, Seyed A. Sharif[1] MD, J. Stuart Nelson[1,2,3] MD,PhD, Kristen M. Kelly[1,2] MD, that might pose or create a conflict of interest with the information presented in this article.

David J Cuccia, Ph.D. and Anthony J. Durkin, Ph.D. are co-Founders of Modulated Imaging, Inc which developed the Spatial Frequency Domain Imaging device used here as part of the NIH/NCRR funded Laser Microbeam and Medical Program (LAMMP). DJC and AJD having intellectual property rights under US Patent #7729750.

ACKNOWLEDGMENTS

The authors gratefully acknowledge funding provided by the NIH SBIRs 1R43RR030696-01A1, and 1R43RR025985-01, Laser Microbeam, and Medical Program (LAMMP), an NIH/NIBIB Biomedical Technology Center, P41EB05890, the Military Photomedicine Program, AFOSR Grant # FA9550-08-1-0384, and the Beckman Foundation. JSN was supported by the following grants from the National Institutes of Health (AR59244 and AR47551).

REFERENCES

1. Tallman B, Tan OT, Morelli JG, Piepenbrink J, Stafford TJ, Trainor S, Weston WL. Location of port-wine stains and the likelihood of ophthalmic and/or central nervous system complications. Pediatrics 1991;87(3):323–327.
2. Troilius A, Wrangsjo B, Ljunggren B. Patients with port-wine stains and their psychosocial reactions after photothermolytic treatment. Dermatol Surg 2000;26(3):190–196.
3. Kelly KM, Choi B, McFarlane S, Motosue A, Jung B, Khan MH, Ramirez-San-Juan JC, Nelson JS. Description and analysis of treatments for port-wine stain birthmarks. Arch Facial Plast Surg 2005;7(5):287–294.
4. Nelson JS, Kelly KM, Zhao Y, Chen Z. Imaging blood flow in human port-wine stain in situ and in real time using optical Doppler tomography. Arch Dermatol 2001;137(6):741–744.
5. Troilius A, Wardell K, Bornmyr S, Nilsson GE, Ljunggren B. Evaluation of port wine stain perfusion by laser Doppler imaging and thermography before and after argon laser treatment. Acta Derm Venereol 1992;72(1):6–10.
6. Huang YC, Tran N, Shumaker PR, Kelly K, Ross EV, Nelson JS, Choi B. Blood flow dynamics after laser therapy of port wine stain birthmarks. Lasers Surg Med 2009;41(8):563–571.
7. Kuzmina I, Diebele I, Spigulis J, Valeine L, Berzina A, Abelite A. Contact and contactless diffuse reflectance spectroscopy: Potential for recovery monitoring of vascular lesions after intense pulsed light treatment. J Biomed Opt 2011; 16(4):040505.
8. Jung B, Choi B, Durkin AJ, Kelly KM, Nelson JS. Characterization of port wine stain skin erythema and melanin content using cross-polarized diffuse reflectance imaging. Lasers Surg Med 2004;34(2):174–181.
9. Gioux S, Mazhar A, Cuccia DJ, Durkin AJ, Tromberg BJ, Frangioni JV. Three-dimensional surface profile intensity correction for spatially-modulated imaging. J Biomed Opt 2009;14(3):034045.
10. Cuccia DJ, Bevilacqua F, Durkin AJ, Tromberg BJ. Modulated imaging: Quantitative analysis and tomography of turbid media in the spatial-frequency domain. Opt Lett 2005; 30(11):1354–1356.
11. Mazhar A, Dell S, Cuccia DJ, Gioux S, Durkin AJ, Frangioni JV, Tromberg BJ. Wavelength optimization for rapid chromophore mapping using spatial frequency domain imaging. J Biomed Opt 2010;15(6):061716.
12. Attas M, Hewko M, Payette J, Posthumus T, Sowa M, Mantsch H. Visualization of cutaneous hemoglobin oxygenation and skin hydration using near-infrared spectroscopic imaging. Skin Res Technol 2001;7(4):238–245.
13. Randeberg LL, Larsen EL, Svaasand LO. Characterization of vascular structures and skin bruises using hyperspectral imaging, image analysis and diffusion theory. J Biophotonics 2010;3(1–2):53–65.
14. Ayers FR, Cuccia DJ, Kelly KM, Durkin AJ. Wide-field spatial mapping of in vivo tattoo skin optical properties using modulated imaging. Lasers Surg Med 2009;41(6):442–453.
15. Gioux S, Mazhar A, Lee BT, Lin SJ, Tobias AM, Cuccia DJ, Stockdale A, Oketokoun R, Ashitate Y, Kelly E, Weinmann M, Durr NJ, Moffitt LA, Durkin AJ, Tromberg BJ, Frangioni JV. First-in-human pilot study of a spatial frequency domain oxygenation imaging system. J Biomed Opt 2011;16(8): 086015.
16. Pharaon MR, Scholz T, Bogdanoff S, Cuccia D, Durkin AJ, Hoyt DB, Evans GRD. Early detection of complete vascular occlusion in a pedicle flap model using quantitation spectral imaging. Plast Reconstr Surg 2010;126(6):1924–1935.
17. Yafi A, Vetter TS, Scholz T, Patel S, Saager RB, Cuccia DJ, Evans GR, Durkin AJ. Postoperative quantitative assessment of reconstructive tissue status in a cutaneous flap model using spatial frequency domain imaging. Plast Reconstr Surg 2011;127(1):117–130.
18. Gioux S, Mazhar A, Cuccia DJ, Durkin AJ, Tromberg BJ, Frangioni JV. Three-dimensional surface profile intensity correction for spatially modulated imaging. J Biomed Opt 2009;14(3):034045.
19. Zijlstra WG, Buursma A, Meeuwsen-van der Roest WP. Absorption spectra of human fetal and adult oxyhemoglobin, de-oxyhemoglobin, carboxyhemoglobin, and methemoglobin. Clin Chem 1991;37(9):1633–1638.

20. Cuccia DJ. Spatial frequency domain imaging (SFDI): A technology overview and validation of an LED-based clinic friendly device. In: Douglass MR, Oden PI, editors. Emerging digital micromirror device based systems and applications IV. San Francisco, CA: SPIE; D 2012. pp. 825405–825406.
21. Mazhar A, Sharif SA, Saggese S, Choi B, Cuccia DJ, Durkin AJ. Implementation of an LED-based clinical spatial frequency domain imaging system. In: Douglass MR, Oden PI, editors. Emerging digital micromirror device based systems and applications IV. San Francisco, CA: SPIE; 2012. pp. 82540A–82547A.
22. Nguyen JQ, Saager RB, Cuccia DJ, Kelly KM, Jakowatz J, Hsiang D, Durkin AJ. Effects of motion on optical properties in the spatial frequency domain. J Biomed Opt 2011;16(12): 126009.
23. Jung B, Kim CS, Choi B, Kelly KM, Nelson JS. Use of erythema index imaging for systematic analysis of port wine stain skin response to laser therapy. Lasers Surg Med 2005; 37(3):186–191.
24. Svaasand LO, Aguilar G, Viator JA, Randeberg LL, Kimel S, Nelson JS. Increase of dermal blood volume fraction reduces the threshold for laser-induced purpura: Implications for port wine stain laser treatment. Lasers Surg Med 2004; 34(2):182–188.
25. Mourant JR, Canpolat M, Brocker C, Esponda-Ramos O, Johnson TM, Matanock A, Stetter K, Freyer JP. Light scattering from cells: The contribution of the nucleus and the effects of proliferative status. J Biomed Opt 2000;5(2): 131–137.
26. Yudovsky D, Durkin AJ. Hybrid diffusion and two-flux approximation for multilayered tissue light propagation modeling. Appl Opt 2011;50(21):4237–4245.
27. Konecky SD, Mazhar A, Cuccia D, Durkin AJ, Schotland JC, Tromberg BJ. Quantitative optical tomography of sub-surface heterogeneities using spatially modulated structured light. Opt Express 2009;17(17):14780–14790.
28. Weber JR, Cuccia DJ, Durkin AJ, Tromberg BJ. Noncontact imaging of absorption and scattering in layered tissue using spatially modulated structured light. J Appl Phys 2009; 105(10):102028.
29. Yudovsky D, Durkin AJ. Spatial frequency domain spectroscopy of two layer media. J Biomed Opt 2011;16(10):107005.
30. Yang O, Cuccia D, Choi B. Real-time blood flow visualization using the graphics processing unit. J Biomed Opt 2011;16(1): 016009.